Organic Electronics 75 (2019) 105375

Contents lists available at ScienceDirect

Organic Electronics

journal homepage: www.elsevier.com/locate/orgel

High-efficiency and low efficiency roll-off in white organic light-emitting diodes employing a novel blue emitter

Ren Sheng[a], Jian Song[a], Asu Li[a], Fujun Zhang[a], Han Zhang[b], Yu Duan[a], Jie Zheng[a], Zhiming Wang[b,**], Ping Chen[a,*]

[a] State Key Laboratory on Integrated Optoelectronics, College of Electronic Science and Engineering, Jilin University, Changchun, 130012, China
[b] State Key Laboratory of Luminescent Materials and Devices, South China University of Technology, Guangzhou, 510640, China

ARTICLE INFO

Keywords:
White OLED
High efficiency
Novel blue fluorescence
Low efficiency roll-off

ABSTRACT

A novel blue fluorophore of 3,40-bis(1-phenyl-phenanthro[9,10-d]-imidazol-2-yl) biphenyl (L-BPPI) was firstly utilized as the blue fluorescent emitter to fabricate highly efficient fluorescent/phosphorescent hybrid white organic light-emitting diodes (WOLEDs). By introducing a mixed interlayer between the blue fluorescent and orange phosphorescent region, two-color WOLED exhibited CIE coordinates close to the equal energy point of (0.33, 0.33) with peak efficiencies of 40.7 cd/A and 26.8 lm/W. And fairly stable white emission spectra were realized owing to the well control of exciton distribution and charge transport balance. Moreover, three-color WOLED was achieved when an ultrathin red phosphorescent emitter was inserted. The result device with reduced efficiency roll-off showed peak efficiencies of 35.3 cd/A and 25.4 lm/W.

1. Introduction

White organic light-emitting diodes (WOLEDs) have become increasingly important due to their potential application in full-color display and solid-state lighting [1–4]. Generally, there are two strategies to generate white light, i.e., the three colors (red, green and blue) and complementary colors (orange and blue) [5]. However, the performance of blue emitters still needs to be improved particularly in terms of efficiency and color purity [6–11]. Although high efficiencies can be achieved by employing full phosphorescent emitter in WOLEDs, the devices often suffer from undesired color coordinates and poor lifetime due to the inappropriate phosphorescent blue emitters. To loosen the bottleneck, hybrid WOLEDs combined blue fluorescent emitters with green-red/orange phosphorescent emitters have garnered growing attraction [12–16]. Actually, the hybrid WOLEDs can not only reach internal quantum efficiency of 100% by the complete utilization of singlet and triplet excitons, but also be able to achieve better electroluminescence (EL) performance due to the pure blue color coordinates and stability of blue fluorophore [17,18].

Recently, some effective hybrid WOLEDs have been reported. For instance, Zhao et al. reported hybrid WOLED with bipolar host exhibited high efficiency of 30.8 cd/A and Commission Internationale de l'Eclairage (CIE) coordinates of (0.43, 0.43) [19]. Wang et al. introduced tris (phenylpyrazole) Iridium as interlayer between yellow phosphorescence emission layer and blue fluorescence emission layer, the hybrid WOLED exhibited peak current efficiency of 21.0 cd/A and low efficiency roll-off [20]. However, the CIE coordinates of these devices are still far from the equal-energy white point of (0.33, 0.33) due to the unsatisfying color purity of blue emitters (i. e, the criterion for a blue emitter is set as $x + y < 0.30$ by National Television System Committee (NTSC)) such as p-bis(p-N,N-diphenyl-amino-styryl) benzene (DSA-Ph) or 2,2′,7,7′-tetrakis(2,2-diphenylvinyl)spiro-9,9′-bifluorene (Spiro-DPVBi), which are difficult to satisfy the requirement of lighting applications [21]. Recently, a novel blue fluorescence material of 3, 40-bis(1-phenyl-phenanthro[9,10-d]-imidazol-2-yl)biphenyl (L-BPPI) with high triplet level was demonstrated by tuning the substituted position on the biphenyl from para- to meta-coupling. The non-doped blue OLED based on L-BPPI exhibited stable pure blue emission and balanced charge injection, revealing its potential to prepare hybrid WOLED as a non-doped blue emitter [21].

In this work, two-color and three-color hybrid WOLEDs were fabricated successfully by using blue fluorescent material of L-BPPI. By employing of mixed interlayer instead of an uniform interlayer between orange doped layer and blue non-doped layer, the two-color WOLED exhibited CIE coordinates close to the equal energy point of (0.33, 0.33) with fairly stable white emission spectra. And peak efficiency of

* Corresponding author.
** Corresponding author.
E-mail addresses: wangzhiming@scut.edu.cn (Z. Wang), pingchen@jlu.edu.cn (P. Chen).

https://doi.org/10.1016/j.orgel.2019.105375
Received 18 June 2019; Received in revised form 22 July 2019; Accepted 23 July 2019
Available online 24 July 2019
1566-1199/

40.7 cd/A (26.8 lm/W) was realized due to the well control of exciton distribution and balanced charge carriers transport. Furthermore, an ultrathin red phosphorescent emission layer was introduced to realize three-color WOLED. The result device showed a peak efficiency of 35.3 cd/A (25.4 lm/W) and low efficiency roll-off with broad emission spectrum coverage. In addition, non-doped blue OLED based on L-BPPI was optimized, revealing its comparative performance compared to that of universal blue fluorescence materials.

2. Experimental

The devices were fabricated on cleaned glass substrates precoated by indium tin oxide (ITO) with a sheet resistance of 20 Ω per square. ITO glasses were cleaned with acetone, methanol, and deionized water successively, followed by a degreaser in an ultrasonic solvent. Molybdenum (VI) Oxide (MoO_3) served as hole injection layer. 4,4′,4"_tris(N-carbazolyl)-triphenylamine (TCTA) with high triplet energy and good hole transport property was used as the hole transport layer (HTL). 1,3,5-Tri[(3-pyridyl)-phen-3-yl]benzene (TmPyPB) was used as the electron transport layer (ETL). 4,40_N,N0_dicarbazole-biphenyl (CBP) with bipolar property was used as host material. L-BPPI and iridium(III) bis(4-phenylthieno-[3,2-c]pyridinato-N,C20) acetylacetonate (PO-01) acted as the blue fluorescence materials and orange phosphorescent materials. Finally, 1 nm Liq covered by 100 nm Al was used as cathode. All organic and metal layers were loaded into thermal vacuum evaporation chamber with a pressure of 3×10^{-4} Pa. Transport materials and L-BPPI were deposited at a rate of 0.1–0.2 nm/s, while PO-01 was grown at the rate of 0.02 Å/s. Electroluminescent (EL) spectra and CIE coordinates of the devices were simultaneously measured by a PR655 spectroscan spectrometer. The current-voltage and luminance-voltage characteristics were recorded with combining the spectrometer with a programmable Keithley 2400 voltage-current source.

3. Results and discussion

Recently, the wholly aryl-substituted phenanthroimidazole (WAPI), an efficient blue emitter block, has attracted tremendous attention due to the simplicity of its synthesis, its excellent thermal properties, high fluorescence quantum yields (reference) and potential “bipolar” properties. As an important derivative, L-BPPI exhibited stable blue emission and good performance in non-doped devices by the optimization of coupling mode from para-linkage to meta-one. The balanced charge injection and transformation ability with proper triplet level might be the main reason, which was benefit to preparing hybrid WOLED as non-doped blue emitter [21].

For OLED incorporating the novel blue fluorophore, finding suitable host material to prevent reverse energy transfer from dopants to host is generally difficult. Therefore three blue devices used L-BPPI are fabricated based on non-doped technology as follow: ITO/MoO_3/TCTA (50 nm)/L-BPPI (X) nm/TmPyPB (50-X) nm/Liq (0.8 nm)/Al, here X = 10, 25, 35, corresponding to device B_1, B_2, and B_3, respectively. Fig. 1 shows the EL characteristics of devices. All of four devices show pure blue emission peak round 440 nm with CIE coordinates of (0.16, 0.10 ± 0.01) as shown in Fig. 1 (d). These values are well agree with the requirement of NTSC standard blue CIE coordinates of ($x + y < 0.30$), revealing high color purity. Device B_1 with 10 nm thickness of blue emission layer shows higher efficiency than other devices. The maximum efficiency achieves 3.82 cd/A (2.89 lm/W), which is more than five times higher than that of previous report (0.68 cd/A). Meanwhile, high luminance of 7033 cd/m^2 and turn-on of 3.3 V are realized, implying that L-BPPI exhibits a comparative performance compared to those of universal blue fluorescence materials [22,23]. More than that, it is worthy mention that as X rises, the current densities of these devices show an obvious increase. This phenomenon demonstrates L-BPPI possesses superior charge carriers transport property, revealing its potential to be the non-doped blue emission layer or the host materials in the WOLED.

White light emission requires the utilization of both blue fluorescence from L-BPPI and the complementary orange phosphorescence from PO-01. Owing to the higher triplet energy level of L-BPPI (3.1 eV) than that of PO-01 (2.2 eV), an effective triplet exciton confinement could be reached to utilize the generated triplet for orange emission. WOLED can be obtained by single emission layer structure, which employs blue emission from singlet excitons on L-BPPI host and orange emission from triplet excitons on the PO-01 dopant. However, the device often requires ultra-low concentration of phosphorescent dopant to separation of singlet excitons, which is difficult to be fabricated accurately and always results in poor spectra stability [24]. Therefore, the structures of separated phosphorescent emission layer and fluorescent emission layer are designed as follow: ITO/MoO_3 (2 nm)/TCTA (50 nm)/CBP: 8% PO-01 (Y nm)/CBP (4 nm)/L-BPPI (10 nm)/TmPyPB (30 nm)/Liq (0.8 nm)/Al. Here Y is chosen as 2, 5, 10, 15, corresponding to devices A-D, as show in Fig. 2 (a). The 4 nm CBP interlayer is used to separate non-doped L-BPPI layer and PO-01 layer to realize their own efficient emission. Fig. 2 (b) shows the normalized spectra of four devices at 7 V. It is clear that four devices show two emission peaks at 440 nm and 560 nm, originating from L-BPPI and PO-01, respectively. The relative intensity of the blue emission decreases compared to the orange emission as x increases, which means more excitons are trapped or harvested by PO-01 molecules in orange layer. It is clear that the device C and D deviate from WOLEDs due to the negligible blue emissions.

The current density-voltage and luminance-voltage characteristics of devices A-D are shown in Fig. 3 (a). The turn-on voltage increases from 2.83 V to 3.02 V. And current density reduces from device A to device D, which means more holes are tapped by PO-01 due to the lower HOMO level of PO-01 (5.1 eV) compared to that of CBP (6.0 eV) as shown in Fig. 2 (a). Fig. 3 (b) shows the current efficiency-luminance and power efficiency-luminance characteristics of four devices. It can be seen that efficiencies increase obviously due to the increasing of efficient orange emission. Meanwhile, device A exhibits efficiencies of 27.5 cd/A and 19.4 lm/W. While peak efficiencies of 35.7 cd/A and 27.0 lm/W are obtained in device B with 5 nm orange emission layer.

The stability of EL spectra is also one of the key factors to evaluate the performance of WOLED. Fig. 3 (c) and (d) exhibit normalized spectra of device A and B at different luminance. We can see that the relative intensity of L-BPPI increases clearly with the increasing luminance. The strong dependence of EL spectra on luminance is arisen from the imbalanced charge carriers transport between orange emission layer and blue emission layer. It should be note that holes mobility show stronger electric field dependence in CPB neat film than electrons [25]. Hence as the driving voltage increases, more holes pass through CBP interlayer and inject from orange layer to blue layer, causing the recombination region shift towards blue emission layer and improved blue emission.

From the results above, we note that although CBP possesses bipolar transport property and frequently acts as universal interlayer, whereas it is inadequate to be the interlayer in our devices due to the unmatched charge transport property with L-BPPI. Therefore, to obtain stable white emission spectra, it is essential to further improve charge transport balance by introducing a mixed interlayer to manipulate charge carriers. Then four devices are fabricated by using interlayer with different mixed radios as the structure of ITO/MoO_3 (2 nm)/TCTA (50 nm)/CBP: 8% PO-01 (5 nm)/TCTA: TmPyPB (4 nm)/L-BPPI (10 nm)/TmPyPB (30 nm)/Liq (0.8 nm)/Al, the mixed ratio of TCTA to TmPyPB are modulated by 4: 1, 2: 1, 1: 2, 1: 6, corresponding to devices W_1–W_4. Fig. 4 (a) shows the normalized spectra of four devices at 6 V. Note that the relative intensity of orange emission clearly increases with the increasing of TmPyPB doping concentration in four devices, which can be attributed to the shift of recombination region towards hole transport layer. The trends suggest that holes and electrons can be well managed

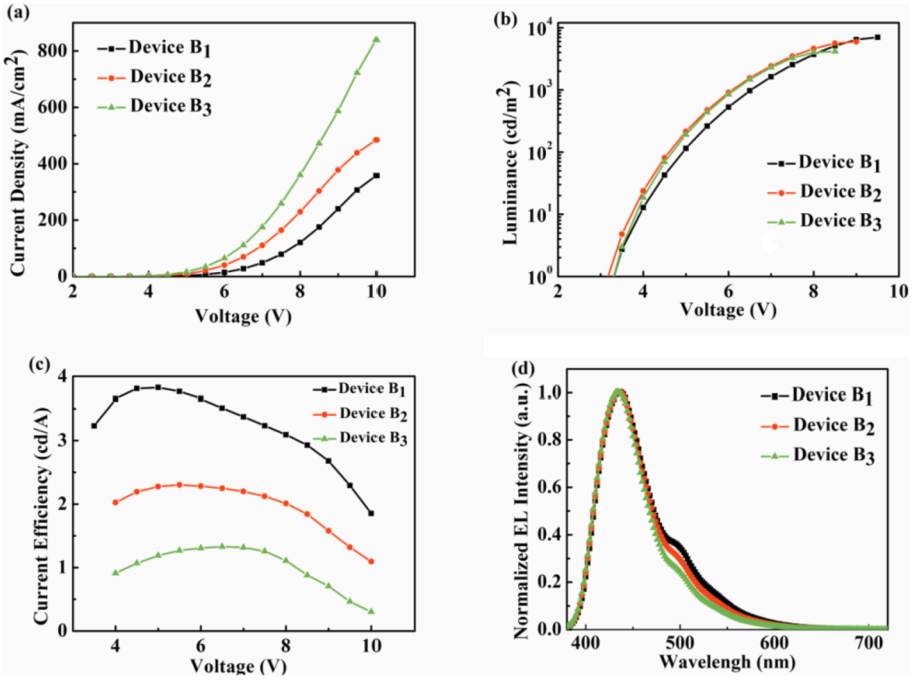

Fig. 1. The current density-voltage characteristics (a), luminance-voltage characteristics (b), current efficiency-voltage characteristics (c) and normalized EL spectra of the devices B_1– B_3 at 6 V (d).

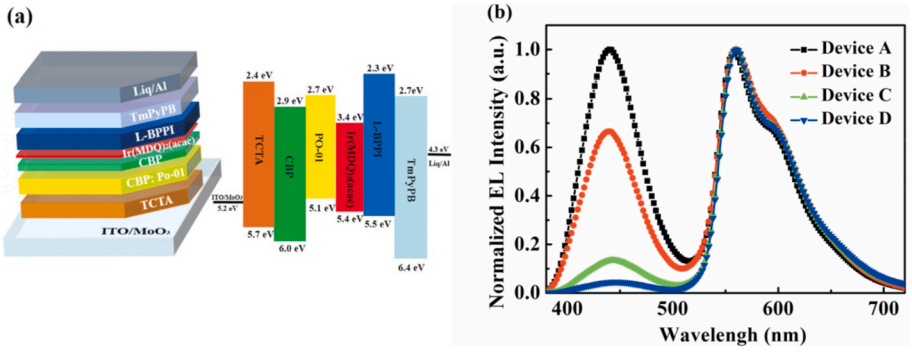

Fig. 2. The structures of the OLEDs and the detailed energy level diagram of the materials (a) and normalized EL spectra of the devices A-D at 7 V (b).

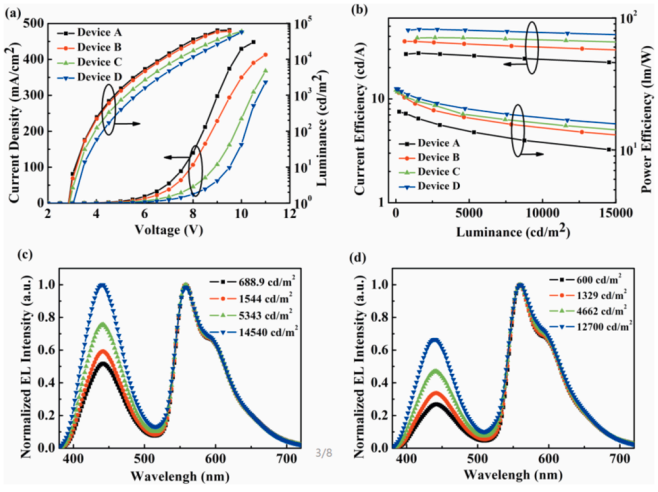

Fig. 3. The current density-voltage and luminance-voltage characteristics (a) and the current efficiency-luminance and power efficiency-luminance characteristics (b) of devices A-D. The normalized EL spectra of the devices A (c) and B (d) at different luminance.

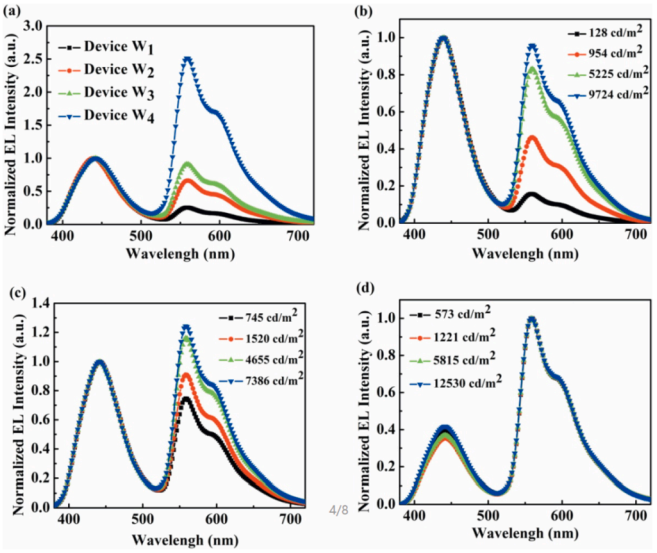

Fig. 4. Normalized EL spectra of the devices W_1–W_4 at 6 V (a) and normalized EL spectra of the devices W_2–W_4 at different luminance (b–d).

by employing mixed interlayer: As the TCTA concentration increases in mixed layer, holes can cross interlayer and reach blue emission layer easily, leading to increased blue emission. On the contrary, as the TmPyPB concentration increases, electrons can be injected into orange emission layer easily, leading to the increase of the orange emission. Therefore, the interlayer should serve as a charge switch, which can manipulate the EL performance of devices by adjusting the mixed ratio.

Fig. 4 (b)–(d) depict the normalized EL spectra of the devices W_2 -W_4 at different luminance. As can be seen, device W_2 and W_3 exhibit enhanced orange emission as the luminance increases, revealing contrary phenomenon compared to device A and B. We deduce that the charge transport property of mixed interlayer is different from that of CBP interlayer: thanks to the fact that the electron mobility of TmPyPB ($\sim 10^{-3}\,cm^2\,V^{-1}\,s^{-1}$) is one order of magnitude higher than that of CBP ($\sim 10^{-4}\,cm^2\,V^{-1}\,s^{-1}$),the mixed interlayer prefer to transport electrons rather than holes. Therefore, electron injection from blue emission layer to orange emission layer is favored with the increasing luminance, resulting in exciton recombination region shift to orange emission layer and enhanced orange emission. With the increasing ratio of TmPyPB in mixed interlayer, the spectra become stable in device W_4 as shown in Fig. 4 (d). We conclude that with increasing doping level of TmPyPB, mixed interlayer shows better electron transport property, which could restrict holes injection to the blue emission layer. In this case, the enhanced electron injection from blue layer to orange layer compensates the increased hole injection from orange layer to blue layer as voltage increases, inducing balanced charge carriers transport and good color stability. As can be seen, with the luminance increasing, the variation CIE coordinates of device W_4 is only (0.014, 0.018) from 573 cd/m^2 to 12530 cd/m^2, revealing a stable white emission spectra. Particularly, device W_4 shows balanced orange and blue emission with CIE coordinates of (0.35, 0.33) at 5 V, which is close to the equal-energy white point of (0.33, 0.33).

Fig. 5 (a) shows the current density-voltage and luminance-voltage characteristics of four devices. The current densities are reduced from device W_1 to device W_4, originating from the reduced hole current density due to the increasing concentration of TmPyPB in the interlayer. The device W_4 shows the turn-on voltage of 3.09 V and maximum luminance of 33720 cd/m^2. The current efficiency-luminance and power efficiency-luminance characteristics of four devices are shown in Fig. 5 (b). Note that the efficiencies increase obviously as the enhancement of TmPyPB doping level. For device W_4 with high TmPyPB proportion in mixed interlayer, more electrons can pass through the interlayer and reach to the orange emission layer. In this case, both singlets and triplets can be harvested by PO-01, resulting in higher efficiencies.

As shown in Table 1, device W_4 shows a peak efficiency of 40.7 cd/A, which is 12% higher than that of device B, indicating that the adjusted mixed interlayer plays an important role in optimizing the distribution of excitons. Moreover, all of four devices show extremely low efficiency roll-off. For device W_4, current efficiency maintain 38.1 cd/A at 5000 cd/m^2 to 35.2 cd/A at 10000 cd/m^2, corresponding to the roll-off of 6.3% and 13.5%. The suppressed efficiency roll-off is attributed to the reduced excitons pileup by following reasons: Firstly, charge carriers can transport between two emission layers without any energy barriers owing to well matched energy levels. And then, the bipolar interlayer structure manages the charge transport between two emission layers, suppressing the efficiency roll-off. Moreover, L-BPPI shows good charge carriers transport property, extending the distribution region of excitons to reduce the triplet-triplet quenching process.

Table 1
Performance of devices W_1–W_4. $\mathbf{V_{on}}$: Turn-on voltage of the devices. ***CE*max/5000/10000 (cd/A)**: maximum current efficiency, current efficiency at 5000 cd/m^2, current efficiency at 10000 cd/m^2; ***PE*max/5000/10000 (lm/W)**: maximum power efficiency, power efficiency at 5000 cd/m^2, power efficiency at 10000 cd/m^2; ***CIE(x, y)*:**CIE coordinates at 1000 cd/m^2.

	V_{on}	*CE*max/5000/10000	*PE*max/5000/10000	*CIE(x, y)*
Device W_1	3.02	16.4/11.8/14.6	8.8/7.8/8.6	(0.22, 0.15)
Device W_2	3.03	21.4/20.0/21.2	12.5/12.3/11.8	(0.29, 0.25)
Device W_3	3.07	24.2/24.0/23.9	16.7/15.5/13.9	(0.31, 0.27)
Device W_4	3.09	40.7/38.1/35.2	26.8/20.8/16.8	(0.35, 0.33)

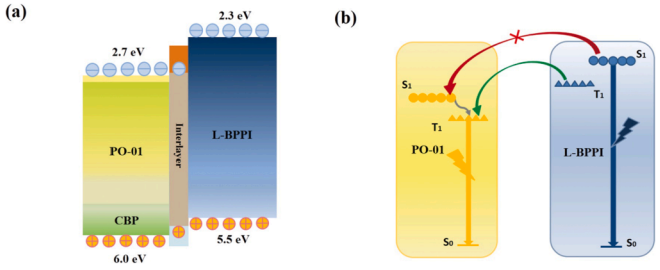

Fig. 6. The charge transport mechanism (a) and the singlet states (S_1) and triplet states (T_1) of materials and exciton transfer mechanism in WOLEDs (b).

The energy transfer mechanism is shown in Fig. 6. Here, singlet diffusion radius (R_S) and triplet diffusion radius (R_T) have been taken into consideration. It is commonly known that Rs is limited to 3 nm [26], suggesting that the singlets of L-BPPI can't be transferred to the orange emission layer by the Förster energy transfer due to the 4 nm of the interlayer in our devices. Therefore, all singlet exciton in L-BPPI can decay radiatively without energy losses. On the other hands, R_T can be up to 100 nm and Dexter energy transfer between triplets and triplets is efficient even with 10 nm [26]. This indicates the triplets of L-BPPI can easily diffuse to the adjacent PO-01 layer and transfer to the triplets of PO-01 by the Dexter energy transfer, preventing triplet energy loss.

Encouraged by the excellent color stability based on complementary-color devices, we further insert an ultrathin layer of Ir

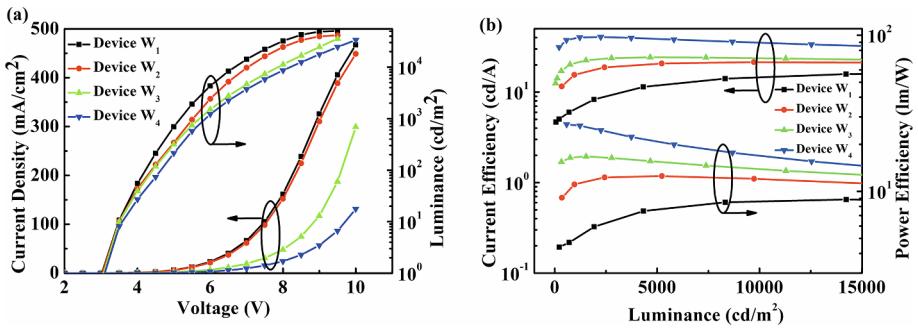

Fig. 5. The current density-voltage and luminance-voltage characteristics of devices W_1–W_4 (a), the current efficiency-luminance and power efficiency-luminance characteristics of devices W_1–W_4 (b).

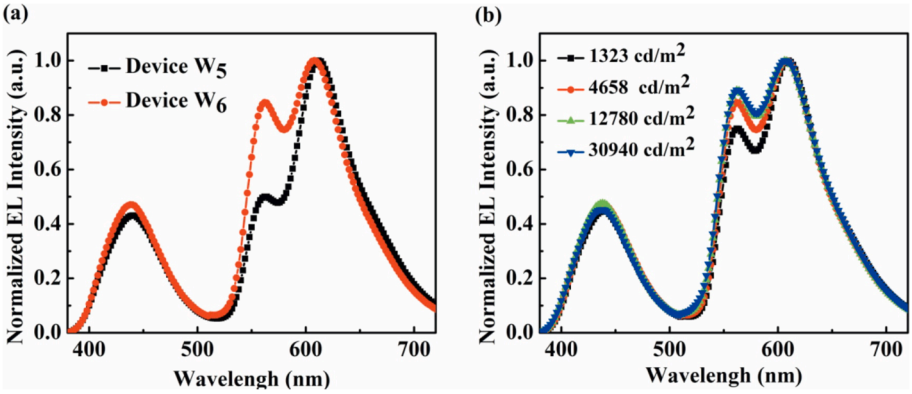

Fig. 7. Normalized EL spectra of devices W_5 and W_6 at 7 V (a) and normalized EL spectra of the devices W_6 at different luminance (b).

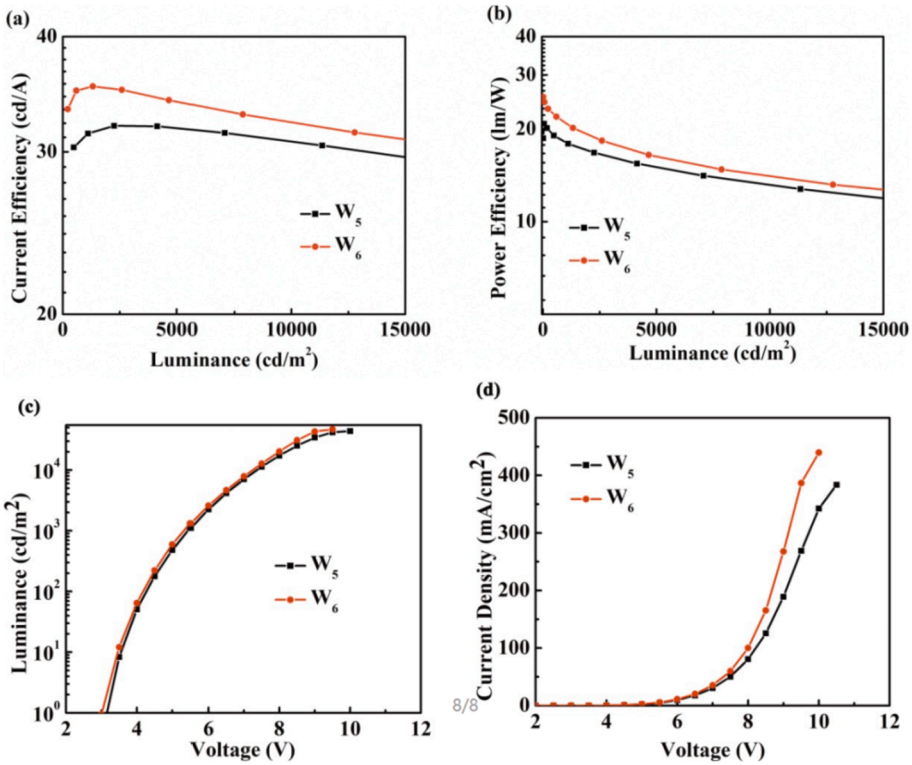

Fig. 8. The current efficiency-luminance (a), power efficiency-luminance characteristics of devices (b), the luminance-voltage (c) and current density-voltage characteristics of devices W_5–W_6 (d).

Table 2
Performance of devices W_5 and W_6. **CRI**: color rendering index at 1000 cd/m^2.

	V_{on}	CE(cd/A)max/5000/10000	PE(lm/W)max/5000/10000	CIE(x, y)	CRI
Device W_5	3.15	32.0/31.6/30.6	20.8/14.9/12.9	(0.45, 0.26)	54
Device W_6	3.01	35.3/33.8/32.4	25.4/16.1/13.8	(0.43, 0.30)	63

$(MDQ)_2(acac)$ into the interface of orange emission layer/interlayer (device W_5) and interlayer/blue emission layer (device W_6) based on the structure of device W_4 to fabricate three-color (red/orange/blue) WOLEDs. Fig. 7 (a) shows the normalized EL spectra of the devices W_5 and W_6 at voltage of 7 V. As we can see, two devices show three emission peaks from L-BPPI, PO-01 and $Ir(MDQ)_2(acac)$, respectively. The weak intensity of orange emission in device W_5 can be attributed to the efficient energy transfer from PO-01 to $Ir(MDQ)_2(acac)$, while Förster energy transfer could be suppressed by the 4 nm of interlayer in device W_6. Fig. 7 (b) depicts the normalized EL spectra of the device W_6 at different luminance. Clearly to see the relative intensity of orange emission become stable with increasing luminance, arising from the emission site saturation of 0.08 nm $Ir(MDQ)_2(acac)$ layer, and thus broaden the emission spectrum coverage. The EL characteristics of the two white devices are shown in Fig. 8 and Table 2. Device W_6 presents a small CIE coordinates variation from (0.428, 0283) to (0.431, 0.325) within the luminance increasing from 1323 cd/m^2 to 12780 cd/m^2. The maximum current efficiency of the device W_6 is 35.3 cd/A, and slightly decreases to 33.8 cd/A at 5000 cd/m^2, 32.4 cd/A at 10000 cd/m^2, showing an excellent efficiency roll-off.

4. Conclusion

In summary, we have successfully demonstrated highly efficient white OLEDs based on a blue fluorophore of L-BPPI. The complementary-color white device achieves CIE coordinates of (0.35, 0.33) at 1000 cd/m^2 with fairly stable white emission spectra and peak efficiencies of 40.7 cd/A and 26.8 lm/W. By further inserting an ultrathin red phosphorescent emitter into complementary-color WOLED, three-color WOLED with peak efficiency of 35.3 cd/A and low efficiency roll-off is realized. The excellent performance can be attributed to the well control of exciton recombination region location by the employment of mixed interlayer and superior charge carriers transport property of L-BPPI.

Acknowledgement

The work was funded by the Project of Science and Technology Development Plan of Jilin Province (20190302011GX, 20190701023GH), National Natural Science Foundation of China (61675088, 61675089).

References

[1] S.R. Forrest, Nature 428 (2004) 911.
[2] K. Leo, S. Reineke, F. Lindner, G. Schwartz, N. Seidler, K. Walzer, B. Lussem, Nature 459 (2009) 234.
[3] A. Misra, P. Kumar, M.N. Kamalasanan, S. Chandra, Semicond. Sci. Technol. 21 (2006) R35.
[4] B.W. D'Andrade, S.R. Forrest, Adv. Mater. 16 (2004) 1585.
[5] T. Peng, Y. Yang, H. Bi, Y. Liu, Z. Hou, Y. Wang, J. Mater. Chem. 21 (2011) 3551.
[6] S.J. Su, E. Gonmori, H. Sasabe, J. Kido, Adv. Mater. 20 (2008) 4189.
[7] Q. Wang, J.Q. Ding, D.G. Ma, Y.X. Cheng, L.X. Wang, F.S. Wang, Adv. Mater. 21 (2009) 2397.
[8] Q. Wang, J.Q. Ding, D.G. Ma, Y.X. Cheng, L.X. Wang, X.B. Jing, F.S. Wang, Adv. Funct. Mater. 19 (2009) 84.
[9] T. Peng, K. Ye, Y. Liu, L. Wang, Y. Wu, Y. Wang, Org. Electron. 12 (2011) 1914.
[10] S. Reineke, F. Lindner, G. Schwartz, N. Seidler, K. Walzer, B. Lüssem, K. Leo, Nature London 459 (2009) 234.
[11] T. Nakayama, K. Hiyama, K. Furukawa, H. Ohtani, J. Soc. Inf. Disp. 16 (2008) 231.
[12] X. Lia, X. Ouyang, M. Liua, Z. Ge, J. Peng, Y. Cao, S. Su, J. Mater. Chem. C. 3 (2015) 9233.
[13] P. Chen, Q. Xue, W. Xie, Y. Duan, G. Xie, Y. Zhao, J. Hou, S. Liu, L. Zhang, B. Li, Appl. Phys. Lett. 93 (2008) 153508.
[14] C. Ho, M. Lin, W. Wong, W. Wong, C.H. Chen, Appl. Phys. Lett. 92 (2008) 083301.
[15] J. Ye, Z. Chen, Fe An, M. Sun, H. Mo, X. Zhang, C. Lee, ACS Appl. Mater. Interfaces 6 (2014) 8964.
[16] N. Sun, Q. Wang, Y. Zhao, Y. Chen, D. Yang, F. Zhao, J. Chen, D. Ma, Adv. Mater. 26 (2014) 1617.
[17] X. Liu, C. Zheng, M. Lo, J. Xiao, Z. Chen, C. Liu, C. Lee, M. Fung, X. Zhang, Chem. Mater. 25 (2013) 4454.
[18] J. Ye, J. Zheng, M. Ou, S. Lee, Adv. Mater. 24 (2012) 3410.
[19] F. Zhao, Z. Zhang, Y. Liu, Y. Dai, J. Chen, D. Ma, Org. Electron. 13 (2012) 1049.
[20] X. Wang, S. Zhang, Z. Liu, S. Yue, Z. Zhang, Y. Chen, G. Xie, Q. Xue, Y. Zhao, S. Liu, J. Lumin. 137 (2013) 59.
[21] Z. Wang, Y. Feng, H. Li, Z. Gao, X. Zhang, P. Lu, P. Chen, Y. Ma, S. Liu, Phys. Chem. Chem. Phys. 16 (2014) 10837.
[22] Y. Li, Y. Liu, W. Bu, Chem. Mater. 12 (2000) 2672.
[23] C. Huang, T. Meen, K. Liao, J. Phys. Chem. Solids 70 (2009) 765.
[24] X. Li, X. Ouyang, M. Liua, Z. Ge, J. Penga, Y. Cao, S. Su, J. Mater. Chem. C. 3 (2015) 9233.
[25] N. Matsusue, Y. Suzuki, H. Naito, Jpn. J. Appl. Phys. 44 (2005) 3691.
[26] X. Liu, W. Chen, H. Chandran, J. Qing, Z. Chen, X. Zhang, C. Lee, ACS Appl. Mater. Interfaces 8 (2016) 26135.